Physica A 630 (2023) 129254

Contents lists available at ScienceDirect

Physica A

journal homepage: www.elsevier.com/locate/physa

A random spatio-temporal model for the dynamics of Candida Auris in Intensive Care Units with regular cleaning

Carlos Andreu-Vilarroig, Juan-Carlos Cortés, Cristina-Luisovna Pérez *, Rafael-Jacinto Villanueva

Instituto de Matemática Multidisciplinar, Universitat Politècnica de València, Valencia, Spain

ARTICLE INFO

Keywords:
Candida Auris
Spatio-temporal biological growth model
Randomized Fisher
Kolmogorov–Petrovsky–Piskunov PDE
Model calibration with noise

ABSTRACT

Candida Auris is a pathogen that can express multiple virulence factors and is considered a significant menace to the Intensive Care Unit environment. In this work, we propose to model its growth with a computationally randomized Fisher Kolmogorov–Petrovsky–Piskunov partial differential equation. We calibrate the model using *in vitro* growth data and provide statistical features. We also evaluate the efficacy of a regular and uniform cleaning strategy with vaporized hydrogen peroxide to control Candida Auris' population in ICUs.

1. Introduction

The antimicrobial resistance (AMR) exhibited by certain strains of pathogens not only hinders the management of their population through the use of antimicrobial drugs in healthcare facilities but also presents a significant danger to the worldwide population. Recently, the World Health Organization (WHO), the United Nations General Assembly, and other organizations have recognized AMR as one of the ten major global public health challenges faced by humanity [1]. For the past five decades, there has been a persistent lack of action in addressing this issue. In numerous influential scientific studies, researchers recognize the significant progress made in public health as a result of antibiotic therapies. However, they also caution against the excessive prescription of antibiotics and their overuse in the food industry, highlighting the need for better control and regulation in these areas [2–4].

Candida Auris (CA) is one of such pathogens. In 2009, Japanese and South Korean patients were the first to be diagnosed with CA infection [5,6]. It has since rapidly spread around the world and is now present in more than 30 countries. The four major clades of this yeast are located in Africa, South America, East Asia, and South Asia [7]. Like many of the microorganisms of its family, CA is able to colonize human body parts such as skin and mucous membranes. Its optimal growth temperature is 37–40 °C, but its population can continue to grow even at temperatures of up to 45 °C [5]. This pathogen can cause both superficial candidiasis and invasive infections such as intra-abdominal candidiasis, chronic otitis media, and bloodstream infections. These complications are more common in severely ill and immunosuppressed patients who have been admitted to the Intensive Care Unit (ICU) [8]. In addition, CA can survive on plastic surfaces, which are commonly found in healthcare settings, for at least two weeks, making it particularly menacing for ICU environments [9].

CA is also capable of expressing various virulence factors, including the creation of biofilms [10], which are communities of microorganisms. Studies have demonstrated that microorganisms present in biofilms are considerably more resistant to medication, partly due to the biofilm cells' capacity to withstand certain antibiotics, such as ampicillin [11]. Moreover, CA is resistant to various cleaning agents typically utilized in healthcare facilities [12]. Due to these microbiological traits, this recently discovered species of

* Corresponding author.
E-mail address: cperdiu@upv.es (C.-L. Pérez).

https://doi.org/10.1016/j.physa.2023.129254
Received 17 July 2023; Received in revised form 11 September 2023
Available online 28 September 2023

yeast has become a significant public health concern in healthcare settings, particularly in the ICU environment on which we focus in this work [12].

The primary manner CA is transmitted in the ICU is through contact between colonized patients and healthcare workers. Since the patients are mostly immobile, they do not usually colonize each other directly. Colonized individuals may shed the virus into their surroundings, but the crucial point lies in the contamination of healthcare workers' hands and reusable diagnostic and observation equipment during their interactions with these patients, making them the primary agents for transmitting the pathogen [13–15].

The current literature available about CA is relatively limited, varied, and new, especially regarding mortality rates. The mortality rates associated with CA vary greatly from one study to the next, depending on both the country and environment in which infected subjects were located. However, the overall mortality rate for CA is significant, with a crude mortality rate[1] ranging from 30% to 72% [17].

Because the ICU population is particularly vulnerable, an uncontrolled CA population poses a significant threat. If appropriate preventive measures are not implemented following the colonization of an ICU patient with CA, it is estimated that the entire ICU would become colonized within a span of 48 hours.[2] Consequently, ICU staff must implement expensive measures to contain the spread of CA, including regular testing of patients, isolating identified colonized patients, and conducting thorough cleaning procedures. Furthermore, this time period is in accordance with surveillance for healthcare-associated infections by CA in Spanish hospitals, including the Hospital General de Valencia. In this hospital, surveillance begins upon a patient's admission and continues weekly throughout their stay. Samples collected are then incubated for 48 h. This 48-hour incubation period is thus the minimum duration required to determine whether a patient has become colonized by CA [18].

Mathematical Modeling is a powerful tool to simulate the dynamics of microorganisms, and, in particular, it can be very useful to model the behavior of CA in the ICU in a cost-efficient manner. Differential equations have been used to model the transmission of CA and the efficiency of control interventions [19]. In the before-mentioned work, it has been found that the optimal control strategy for CA spread is a combination of transmission precaution, molecular-based laboratory methods for the identification of new colonization, and isolation of infected patients. Complementarily, our work will focus on CA's population and its diffusion in space and time. New research on microorganism populations with biofilms has revealed that their diffusion patterns resemble the growth of urban communities [20]. Schematically, an outbreak of a pathogen like CA can be depicted as a bell-shaped surface that spreads through its surroundings in a wave-like manner. Therefore, since our work will focus on the growth and diffusion of CA's population, models used for 2D heat waves seem suitable for representing the extent of contamination in an ICU room at any given moment.

In this work, we propose to model the dynamics of the biological diffusion of CA within an ICU room with the Fisher Kolmogorov–Petrovsky–Piskunov (FKPP) model [21]. We use real-world *invitro* CA growth data from [22] to calibrate our model. However, when we build a model, we cannot account for all complexities of the physical phenomenon in question. The model remains a simplification of the proper biological diffusion of CA since this pathogen not only forms an isolated colony in some spatial point but also is transported by healthcare workers and competes with other microorganisms in its environment. The data also carries uncertainty due to possible measurement errors and equipment limitations. Hence, this work focuses on randomizing the FKPP model to account for the before-mentioned uncertainties that a deterministic model cannot capture. To do so, we use a computational method to describe the FKPP equation as a Random Partial Differential Equation with jumps to model the regular cleaning.

The paper is organized as follows: first, in Section 2, we introduce the FKPP model and the numerical scheme we used to approximate it. Then, in Section 3, we calibrate the model using *in vitro* data. Lastly, in Section 4, we describe the randomization of the model and the corresponding results. The main conclusions of the proposed mathematical modeling are drawn in Section 5.

2. Deterministic model

2.1. Numerical scheme

The FKPP model, a reaction–diffusion equation, can be utilized to depict the progression of population growth over time in a two-dimensional spatial system [21]. In this model, we assume that the diffusion occurs from the source of the CA outward. We are also supposing that diffusion takes place over a homogeneous environment over which diffusion is uniform. This model is independent of the entry and exit of patients in the ICU. The FKPP model is formulated by the following partial differential equation (PDE):

$$\frac{\partial u}{\partial t} = D\left(\frac{\partial^2 u}{\partial x^2} + \frac{\partial^2 u}{\partial y^2}\right) + ru(1-u), \tag{1}$$

where (x, y) are the spatial coordinates in the rectangle $[a, b] \times [c, d] \subset \mathbb{R}^2$, $0 < t < T$ represents the time interval, $u = u(x, y)$ is the density of the pathogen population at the space–time coordinate (x, y, t), $D > 0$ is the diffusion coefficient and $0 \leq r \leq 1$ stands for the growth rate.

The FKPP model can be viewed as a heat diffusion model with an additional heat-source function. More precisely, in this model, the variation of the population density u through time is driven by both the diffusion term, $D\nabla^2 u$ where $\nabla^2 u := \left(\frac{\partial^2 u}{\partial x^2} + \frac{\partial^2 u}{\partial y^2}\right)$ is the

[1] The crude mortality rate is defined by the Centers for Disease Control and Prevention (CDC) as the "total number of deaths during a given time interval" [16].

[2] Private information provided by chief ICU medical personnel (Hospital General de Castellón, Spain).

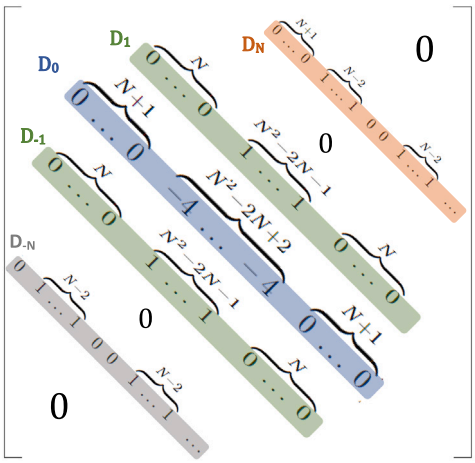

Fig. 1. Schematic representation of matrix A.

Laplacian of u, which models microorganism's expansion on a surface, and the population growth term, $ru(1-u)$, which indicates the amount of CA at a given time and point. We can observe that the population growth term follows the so-called logistic growth. The logistic model is widely used to describe the growth of a population with limited carrying capacity. Therefore, it is natural to use this model for the growth of CA in the ICU environment. We do note that there are alternative growth models, such as linear, Gompertz, etc., that could also be considered, but the logistic model is a good compromise between difficulty and number of parameters to calibrate. A more thorough review of different growth models can be found in [23], [24, Ch 1]. As no closed solution to the FKPP equation is available, one must rely on implementing appropriate numerical schemes to solve it.

We choose to use explicit finite differences with Neumann boundary conditions and adapt the algorithm from [25,26]. We execute the algorithm using *Matlab*, and for simplicity, we assume that $a = c = 0$ and $b = d = 10$. We note that 10 is an arbitrary number we have chosen, and the plane can be built using any different size. To divide the corresponding $[0, 10]^2$ square representing the ICU in two dimensions, we build a 101×101 mesh-grid, where $x \in \{0, 0.1, 0.2, \dots, 10\}$ and $y \in \{0, 0.1, 0.2, \dots, 10\}$, with spatial step $h = 0.1$ in both directions.

We let the time go from 0 to 48 hours with a time step of $k = \min\{0.5, 0.99\frac{h^2}{4D}\}$ so that $k < \frac{h^2}{4D}$ in order to guarantee stability in the numerical scheme [27].

Our numerical scheme, in matrix form, is given by:

$$\begin{aligned} \hat{u}^{(j+1)} &= \frac{kD}{h^2} A\hat{u}^{(j)} + \hat{u}^{(j)} + kr\hat{u}^{(j)} \circ (1 - \hat{u}^{(j)}), \\ \hat{u}^{(j)^\top} &= \left[\hat{u}_{1,1,j} = 0, \hat{u}_{2,1,j}, \hat{u}_{3,1,j}, \dots, \hat{u}_{N,1,j} = 0, \dots, \hat{u}_{1,N,j} = 0, \dots, \hat{u}_{N,N,j} = 0\right], \end{aligned} \tag{2}$$

for $j = 1, \dots, T$, where $\hat{u}$ is the numerical approximation of the solution of (1), A is a $N^2 \times N^2$, $N = 100$ matrix with all zeros except at the main diagonal, D_0, off 1 diagonals, D_{-1}, D_1 and off N diagonals, D_{-N}, D_N as illustrated by Fig. 1. We note that $\circ$ in (2) denotes the Hadamard product (also known as the element-wise product). We will later set the initial condition of the algorithm to be coherent with respect to the data as explained in Section 3.

2.2. Introduction of a cleaning factor

As it is mandatory in ICU settings, trained personnel are assumed to regularly clean the ICU to minimize the spread of pathogens. In order to estimate the effectiveness of cleaning measures to control the population of CA, we incorporate a cleaning factor into our model. We assume that the cleaning is homogeneous (CA at all points of the ICU room gets reduced by the same amount) and regular (it occurs every t_1 hours).

Let $\hat{u}$ be the approximate solution u to the PDE (1) using the above-mentioned numerical scheme (2). Then when cleaning is introduced to the model, the amount of CA in the ICU at every spatial point $(x, y) \in \{0, 0.1, 0.2, \dots, 10\}^2$ on the plane and time instant t is

$$\hat{u}_C(x, y, t) = \begin{cases} (1 - p)\hat{u}(x, y, t), & \text{if } t = nt_1, n = 1, \dots, \text{floor}(\frac{T}{t_1}), \\ \hat{u}(x, y, t), & \text{otherwise,} \end{cases} \tag{3}$$

where $p \in (0, 1)$ is the percent by which the CA is reduced and t_1, $0 < t_1 < T$, represents the period with which the ICU's cleanings are carried out. We note that p can be viewed as the efficacy of the cleaning and is better the closer it is to 1.

Table 1
Evolution of the growth of Candida Auris (CA) measured in absorbance at 600 nm wavelength ($A600$ nm), at different time instants. Observe that $y_{max} = y_{34} = 2.88$, which is used to normalize the data. The normalized data is calculated as $z_i = \frac{y_i}{y_{max}}$, $i = 1, 2, \ldots, 41$.

t (h)	$A600$ nm	t (h)	$A600$ nm	t (h)	$A600$ nm
$t_1 = 3.91$	$y_1 = 0.070$	$t_{15} = 12.55$	$y_{15} = 1.41$	$t_{29} = 27.83$	$y_{29} = 2.80$
$t_2 = 5.76$	$y_2 = 0.10$	$t_{16} = 13.14$	$y_{16} = 1.50$	$t_{30} = 28.81$	$y_{30} = 2.81$
$t_3 = 8.03$	$y_3 = 0.28$	$t_{17} = 13.45$	$y_{17} = 1.63$	$t_{31} = 30.57$	$y_{31} = 2.83$
$t_4 = 9.21$	$y_4 = 0.37$	$t_{18} = 13.76$	$y_{18} = 1.77$	$t_{32} = 33.20$	$y_{32} = 2.86$
$t_5 = 10.30$	$y_5 = 0.52$	$t_{19} = 14.07$	$y_{19} = 1.94$	$t_{33} = 35.25$	$y_{33} = 2.87$
$t_6 = 10.50$	$y_6 = 0.61$	$t_{20} = 15.34$	$y_{20} = 1.97$	$t_{34} = 37.11$	$y_{34} = 2.88$
$t_7 = 10.81$	$y_7 = 0.70$	$t_{21} = 16.23$	$y_{21} = 2.02$	$t_{35} = 40.81$	$y_{35} = 2.87$
$t_8 = 11.11$	$y_8 = 0.80$	$t_{22} = 18.09$	$y_{22} = 2.06$	$t_{36} = 42.57$	$y_{36} = 2.86$
$t_9 = 11.32$	$y_9 = 0.89$	$t_{23} = 19.46$	$y_{23} = 2.16$	$t_{37} = 45.20$	$y_{37} = 2.86$
$t_{10} = 11.62$	$y_{10} = 0.99$	$t_{24} = 20.45$	$y_{24} = 2.25$	$t_{38} = 46.53$	$y_{38} = 2.82$
$t_{11} = 11.93$	$y_{11} = 1.09$	$t_{25} = 22.32$	$y_{25} = 2.44$	$t_{39} = 49.09$	$y_{39} = 2.77$
$t_{12} = 11.94$	$y_{12} = 1.17$	$t_{26} = 23.61$	$y_{26} = 2.55$	$t_{40} = 50.26$	$y_{40} = 2.73$
$t_{13} = 12.14$	$y_{13} = 1.25$	$t_{27} = 24.18$	$y_{27} = 2.68$	$t_{41} = 51.42$	$y_{41} = 2.73$
$t_{14} = 12.44$	$y_{14} = 1.33$	$t_{28} = 26.56$	$y_{28} = 2.78$		

3. Model calibration

3.1. Data

The data we use to calibrate our model is *invitro* growth data from [22]. These measurements come from experimental strains of CA inoculated onto Sarcocystis dextrose agar. These strains were incubated for 48 hours at a constant temperature of 37 °C [22], which is the average human body temperature and within the optimal growth temperature of CA. The measurements are given as the absorbance at 600 nm wavelength ($A600$ nm). While the data may not fully represent CA's growth on plastic surfaces, it better represents its growth in a colonized human. We can thus view it as an average (although it might be overestimating the true average) of the growth rates in the ICU room. We note that this data cannot be used to calibrate the FKPP model directly. Rather, we view it as an estimate of the total amount of CA in the ICU at any given time instant (corresponding to taking the double integral of $\hat{u}$, the numerical solution of Eq. (1), for a fixed t).

The normalized data is calculated as $z_i = \frac{y_i}{y_{max}}$, $i = 1, 2, \ldots, 41$, where $y_{max} = y_{34} = 2.88$ (see Table 1). Note that the data used goes up to $t_{41} = 51.42$ hours. However, we run all simulations for 48 hours to study the growth of CA during the first two days, as this has been indicated (as explained in the Introduction) to be the time it takes for uncontrolled CA to colonize the ICU fully. We also note that, in this data, the growth of CA is logarithmic for $8 - 24$h and stabilizes after 24h [22]. The stabilization after 24h corresponds to the stationary phase during which there is no net growth that occurs when resources are limited [28].

3.2. Calibration: Logistic growth

The growth data from [22], summarized in Table 1, corresponding to points shown in Fig. 2, approximately follows a logistic growth and can be modeled through the logistic growth equation:

$$\frac{\partial u}{\partial t} = ru(1 - u). \tag{4}$$

Note that this equation corresponds to the source term of (1). It has the following closed-form solution:

$$u(t) = \frac{u_0 \exp(rt)}{u_0(\exp(rt) - 1) + 1}, \tag{5}$$

where u_0 is the initial normalized quantity of CA in the ICU, and r is the growth rate of CA. Since we have the explicit expression (5) and data, we can use Nonlinear Least Squares (NLS) to estimate the model parameters u_0 and r. We note that most non-linear models cannot be solved analytically [29], and we thus choose to solve it numerically using the *R* function *nls* [30] from the *stats* package [31]. This function uses, by default, a Gauss–Newton algorithm which iteratively finds the value of the model parameters that minimize the sum of squares of the differences between data and model values obtained according to expression (5) [32, p. 342–348]. Using this function, we get an estimate of the parameters r and u_0 so that Eq. (5) fits the normalized CA growth data $z_i, i = 1, 2, \ldots, 41$. Fig. 2 shows that the resulting estimate aligns closely with the data. The resulting estimated parameters $\hat{u}_0 = 0.01507$ and $\hat{r} = 0.30955$ will allow us to both solve the FKPP numerical scheme and randomize the model.

3.3. Calibration: Initial condition of FKPP

In order to obtain a solution for the FKPP equation (1) using the numerical scheme introduced in Section 2.1, and thus be able to calibrate the model, it is necessary to specify an initial condition (IC) consistent with our previous findings and literature regarding microbial populations. The dynamics of microorganism populations in biofilms have been shown to share structural aspects with

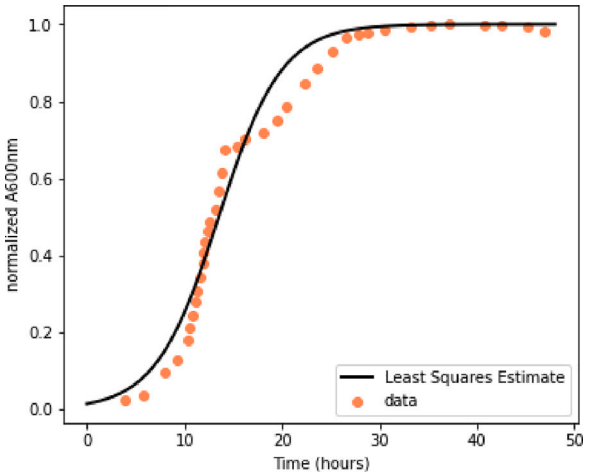

Fig. 2. Normalized data of CA growth (t_i, z_i), $i = 1, 2, \ldots, 41$, compared with the NLS (Nonlinear Least Square) estimate.

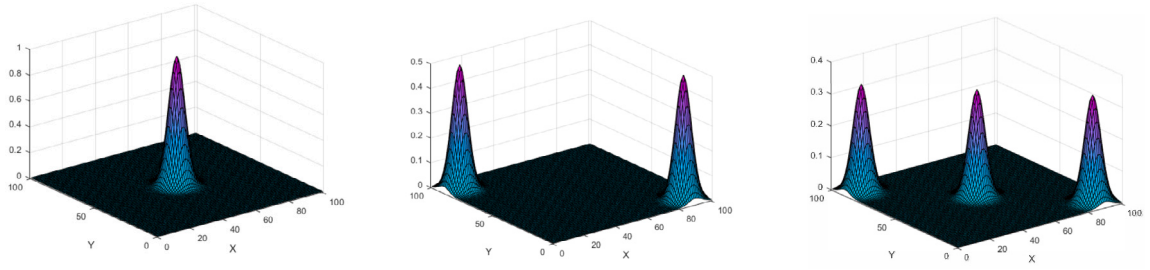

(a) 1 peak. (b) 2 peaks. (c) 3 peaks.

Fig. 3. Initial conditions with varying amounts of peaks.

urbanizations [20]. Based on the definitions provided in [20], we make the assumption that the outbreak of CA is a city (densely populated microcolonies) and resembles a dome structure enclosed within well-defined boundaries [20]. Therefore, the IC should be bell-shaped. For the sake of simplicity, we will set the IC to model an outbreak in the ICU's center. In order for the IC to agree with previous results of the NLS estimate, $u_0 = 0.01507 \approx 10^{-2}$, we set the initial total amount of CA in the ICU, $\int_0^{10}\int_0^{10} u(x, y, 0)\,\mathrm{d}x\mathrm{d}y$, to be around 10^{-2}.

We choose the IC to be $u(x, y, 0) = \exp\{-3\big((x-5)^2 + (y-5)^2\big)\}$. This function is bell-shaped and centered in the middle of our $[0, 10]^2$ ICU with

$$\frac{1}{M}\int_0^{10}\int_0^{10} \exp\{-3\big((x-5)^2 + (y-5)^2\big)\big)\,\mathrm{d}x\mathrm{d}y \approx 1 \times 10^{-2},$$

where the normalizing constant $M := 101.97 = 0.1^2 \sum\sum_{x,y\in\{0.1,0.2,\ldots,10\}} \hat{u}(x, y, 48)$ corresponds to the maximum amount of CA in the ICU plane (this maximum occurs at $t = 48$ h) and 3 is the smallest natural number that makes the integral evaluate at approximately 10^{-2}.

Remark 1. We note that for simplicity, we chose to model only one peak located in the center of the ICU, shown in Fig. 3(a), but one could also decide to generate more peaks that still agree with all the before-mentioned conditions. Two examples are represented in Figs. 3(b) and 3(c), but many other possible variations of IC setups could be proposed.

Remark 2. Note that the values of D and r may vary depending on the initial condition. For example, when the initial outbreak is farther from the center of the ICU plane, it takes slightly longer for the pathogen to grow.

3.4. PSO algorithm to calibrate FKPP parameters

First, we note that the CA growth data [22] gives a total amount of CA at any given time without giving any information about CA's population's distribution in space. It can, therefore, not directly be compared with the FKPP model outputs. We need to define

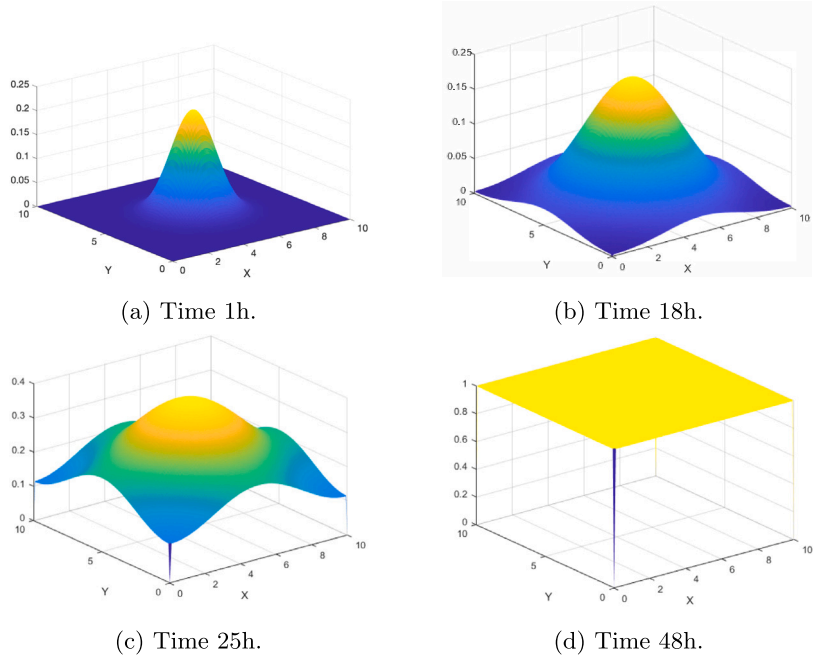

Fig. 4. 3D plots of the FKPP numeric solutions when $\hat{D} = 0.4141$ and $\hat{r} = 0.3539$.

a mapping from our 3D model into 2D so we can compare it to data. This function will take the total amount of CA present in the ICU room at a given time and normalize it so that its range is restricted to $[0, 1]$. We build it in a few steps. First, let F be as follows

$$F(t) := \int_0^{10} \int_0^{10} u(t, x, y)\, \mathrm{d}x\mathrm{d}y,$$

which we estimate in our numerical scheme by

$$\hat{F}(t) := 0.1^2 \sum \sum_{x,y \in \{0,0.1,\ldots,10\}} \hat{u}(x, y, t).$$

Now we will normalize our transformation as well so that

$$f(t) := \frac{1}{M} \hat{F}(t) \tag{6}$$

is the function we will use in this work to compare model outputs to CA's growth data. Now that we have function (6) and the IC defined, we can find pairs of parameters (D, r) that represent our data. To do so, we apply Particle Swarm Optimization (PSO), a bio-inspired optimization algorithm first introduced by Kennedy and Eberhart in 1995 [33]. We define it as the fitness function for the PSO to minimize the Symmetric Mean Absolute Percentage Error (SMAPE), which has been shown to be a good measure of relative error [34]. We opted to utilize SMAPE in our simulations because it does not assign greater importance to larger data values, thus preventing them from excessively influencing the overall solution. The SMAPE we used is defined as:

$$E = \frac{1}{41} \sum_{i=1}^{41} \frac{|z_i - f(t_i)|}{\frac{|z_i| + |f(t_i)|}{2}} \tag{7}$$

where $\{t_1, t_2, \ldots, t_{41}\}$ is the set of times where CA's $A600$ nm was measured, $\{z_1, z_2, \ldots, z_{41}\}$ are the corresponding normalized $A600$ nm measurements collected in Table 1 and f is as defined in (6). The PSO algorithm will provide pairs of (D, r) that minimize the error E as defined in (7). We take the pair of parameters returned from the PSO calibration ran as is later described in Section 4. This solution is $\hat{D} = 0.4141, \hat{r} = 0.3539$, and it is illustrated in Fig. 4. In this plot, we can see how CA colonized the whole room as time goes on until it reaches a value of 1 in all the points of the ICU plane, except the corners. We note that the scale in each plot of the panel of Fig. 4 differs in order to better see the shape of the solution at each time instant illustrated.

4. Random model

4.1. From the deterministic to the random model

So far, we have focused on the dynamics of the growth rate and shape of the pathogen's population in an ICU room by means of a deterministic model. Now, we complete the model by considering uncertainties in its mathematical formulation. It is justified

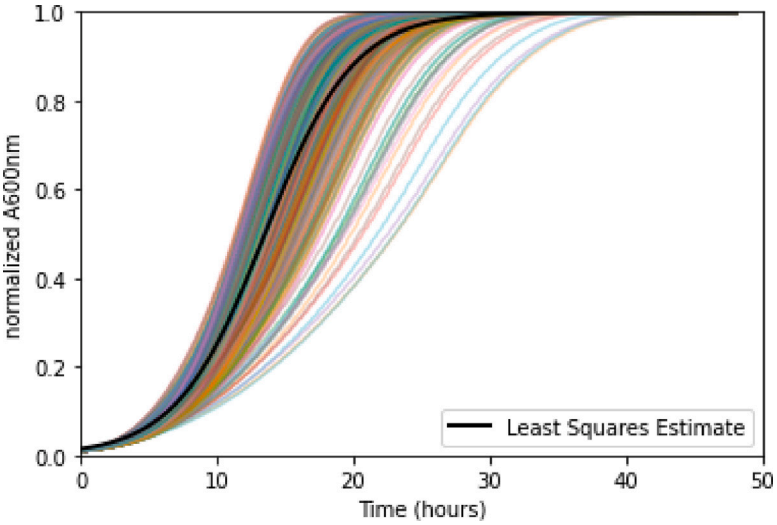

Fig. 5. 591 PSO calibration results with error less than 4. The black line corresponds to the NLS algorithm estimate of (5).

because randomness appears from different sources, such as the lack of knowledge of factors determining the dynamics associated with CA growth, error measurements to collect datasets or samples, etc. Based on these reasons, we propose a randomized version of the FKPP model for pathogens. In dealing with stochastic/random models formulated by partial differential equations, besides calculating, exact or numerically, the solution, the main goal is to compute its statistics, such as the mean and the variance/standard deviation functions. However, a more desirable objective is to determine the first probability density function (1-PDF) of the solution. Because the FKPP model does not have a closed-form solution, we cannot use the Random Variable Transformation method [35–37] to determine the 1-PDF, but we must work with the randomized model computationally.

To do a probabilistic calibration, we perform five calibrations with a maximum of 500 model evaluations in the same way and with the same error that we used for the deterministic calibration in Section 3. This provides us with a total of 2500 model evaluations, which is not a high number of evaluations, but we have to consider the computational cost of the numerical solution of the FKPP model (note that the algorithm has an adaptive time step, $k = \min\{0.5, 0.99\frac{h^2}{4D}\}$, which can be very small for some values of D, making the simulations slower). We order the 2500 evaluations by error.

Now, we are going to select some of the 2500 evaluated sets of parameters such that their model outputs can contain the data and their errors, which is known as capturing the data uncertainty, and later, we will define it more precisely.

To reduce the potential combinations (search space) for the selection algorithm, we need to set an error threshold; we select the model outputs whose evaluations have an error less than the threshold, reducing the eligible model outputs and taking only the closest to the data. To do so, we take the first quantile of all the evaluations previously sorted out by error. We then set the error threshold to be multiples of the first quantile until we have enough evaluations on each side of the NLS estimate and get around 600 simulations in total. This gave us an error threshold of 4. Restricting the error to 4, allowed us to alleviate the computational burden for later algorithms. To be precise, we kept 591 of these sets so that the errors associated are all under 4. Fig. 5 shows the model outputs simulated with the 591 pairs of (D, r). Note that although there are some evaluations that have a greater distance from the NLS estimate in the lower half of the plane, there are more evaluations located in the top part.

The objective now is to select from these 591 model parameters/outputs a subset that will capture as accurately as possible the data uncertainty, that is, when the following two errors are as small as possible at the same time:

(1) The first, denoted as F_{CI}, will control for the size of the 95% confidence interval (CI) of the selected simulations, penalizing the CIs that are too wide;
(2) The second, denoted as F_{IO}, is the so-called inside-outside error and prioritizes simulations where the data lie inside the 95% CI of the simulations.

These errors are orthogonal in the sense that when F_{CI} is big (big 95% CI), F_{IO} will be small (most of the data points will lie inside the 95% CI), and vice versa [38].

It is important to note that here, we face a multi-objective problem, in which we aim at minimizing both objective functions, F_{CI}, and F_{IO}, simultaneously. As a result, the optimization problem does not yield a single solution but rather a set of Pareto-optimal solutions that provides us with a Pareto front [39]. These solutions are not dominated by any other solution in terms of both objectives simultaneously, meaning that any improvement in one objective function would require sacrificing the performance of the other [39].

At this point, we have 591 pairs of parameters $P_i = (D_i, r_i)$ and their corresponding model outputs $f(t_1)^{P_i}, \dots, f(t_{41})^{P_i}, i = 1, 2, \dots, 591$, at the time instants $t_1, \dots, t_{41}$, respectively, that is

$$\begin{array}{cccccccccc} \text{Index} & \text{Parameters} & & & & \text{Output} & & & & \\ 1 & P_1 = (D_1, r_1) & \Theta(1) & = & (& f(t_1)^{P_1}, & f(t_2)^{P_1}, & \dots, & f(t_{41})^{P_1} &), \\ 2 & P_2 = (D_2, r_2) & \Theta(2) & = & (& f(t_1)^{P_2}, & f(t_2)^{P_2}, & \dots, & f(t_{41})^{P_2} &), \\ \vdots & \vdots & \vdots & \vdots & \vdots & \vdots & \vdots & \vdots & & \\ 591 & P_{591} = (D_{591}, r_{591}) & \Theta(591) & = & (& f(t_1)^{P_{591}}, & f(t_2)^{P_{591}}, & \dots, & f(t_{41})^{P_{591}} &), \end{array} \tag{8}$$

where function f is defined in (6).

If we consider $I_h \subseteq I = \{1, \dots, 591\}$ a subset of indexes of I, taking the rows $\Theta(i)$, $i \in I_h$, for each column we can calculate the percentiles 2.5 and 97.5 and denote them as $q^{I_h} = (q(t_1)^{I_h}, \dots, q(t_{41})^{I_h})$ and $Q^{I_h} = (Q(t_1)^{I_h}, \dots, Q(t_{41})^{I_h})$, respectively.

Now, we define here explicitly the errors mentioned above:

$$F_{\text{CI}}(I_h) = \sum_{i=1}^{41} |Q(t_i)^{I_h} - q(t_i)^{I_h}|, \tag{9}$$

$$F_{\text{IO}}(I_h) = \sum_{i=1}^{41} d\left(z_i, [q(t_i)^{I_h}, Q(t_i)^{I_h}]\right), \tag{10}$$

where $\{z_1, \dots, z_{41}\}$ are the normalized $A600$ nm measurements at times $\{t_1, \dots, t_{41}\}$ from Table 1, respectively, and

$$d(p, [a, b]) = \begin{cases} 0, & \text{if } a \le p \le b, \\ \min\{|p - a|, |p - b|\}, & \text{otherwise.} \end{cases} \tag{11}$$

As we mentioned above, these two errors (9)–(10), measure whether the model captures the data uncertainty. Thus, the goal consists of finding a subset $I_{h^*} \subseteq I$, such that the pair $(F_{\text{CI}}(I_{h^*}), F_{\text{IO}}(I_{h^*}))$ will be as small as possible and non-dominated. A discussion about alternatives to error functions (9)–(10) can be found in [40].

To achieve that, we use a selection algorithm based on the multi-objective particle swarm optimization [41] (MOPSO), called MOPSO-selection. This is a multiobjective version of the selection algorithm presented in [42].

1. Parameters of the algorithm.
   - n, the number of particles in MOPSO-selection.
   - k, the number of elements of each particle.
   - $0 < s < k$, number of new elements of a particle that will be included when it is updated.
   - $ITMAX$, the maximum number of iterations of the algorithm.
2. Initialization.
   - Let $I_1, \dots, I_n \subset \{1, \dots, 591\}$ be the set of indexes (particles), where $|I_1| = \cdots = |I_n| = k < 591$.
   - Calculate the particles fitnesses $(F_{\text{CI}}(I_i), F_{\text{IO}}(I_i))$, $i = 1, \dots, n$.
   - We define the local best of each particle as $I_i^{localbest} = \{I_i\}$, $i = 1, \dots, n$.
   - We define the global best $I^{globalbest}$ as the Pareto front of all the local best.
3. STEP 1 (particle update). For $i = 1$ to n.
   - We define the auxiliary set S as the union of the elements of the I_i, the elements of all the $I_i^{localbest}$, and the elements of all the $I^{globalbest}$, and remove the repeated elements.
   - The updated I_i will be make up of $k - s$ elements of S chosen randomly and s elements of {1,...,591} chosen randomly and different from the $k - s$ first, totaling, k elements in the updated I_i.
4. STEP 2 (particle fitness calculation). For $i = 1$ to n, calculate the 2-objective errors $(F_{\text{CI}}(I_i), F_{\text{IO}}(I_i))$ of the updated I_i.
5. STEP 3 (updating the local best and the global best) For $i = 1$ to n.
   - The local best of $I_i^{localbest}$ is updated as the Pareto front of the old local best, adding the updated I_i (with its errors).
   - In the same way, if the local best has been updated, the updated $I^{globalbest}$ is updated as the Pareto front of the old global best, adding the current updated I_i (with its errors).
6. STEP 4 (end criterion) The process finishes when ITMAX iterations have been reached, and the algorithm returns $I^{globalbest}$, the Pareto front with the best non-dominated solutions. Otherwise, go to STEP 1.

The $I^{globalbest}$ returned by the algorithm will contain subsets of k elements of the set $\{1, \dots, 591\}$ whose 2-objective errors, F_{CI} and F_{IO}, are non-dominated.

Because we do not know exactly how many simulations should compose a particle in this algorithm, we let the number of simulations k (number of elements of the indexes subset) vary, setting it to 30, 60, or 90. We also let the number of particles n be

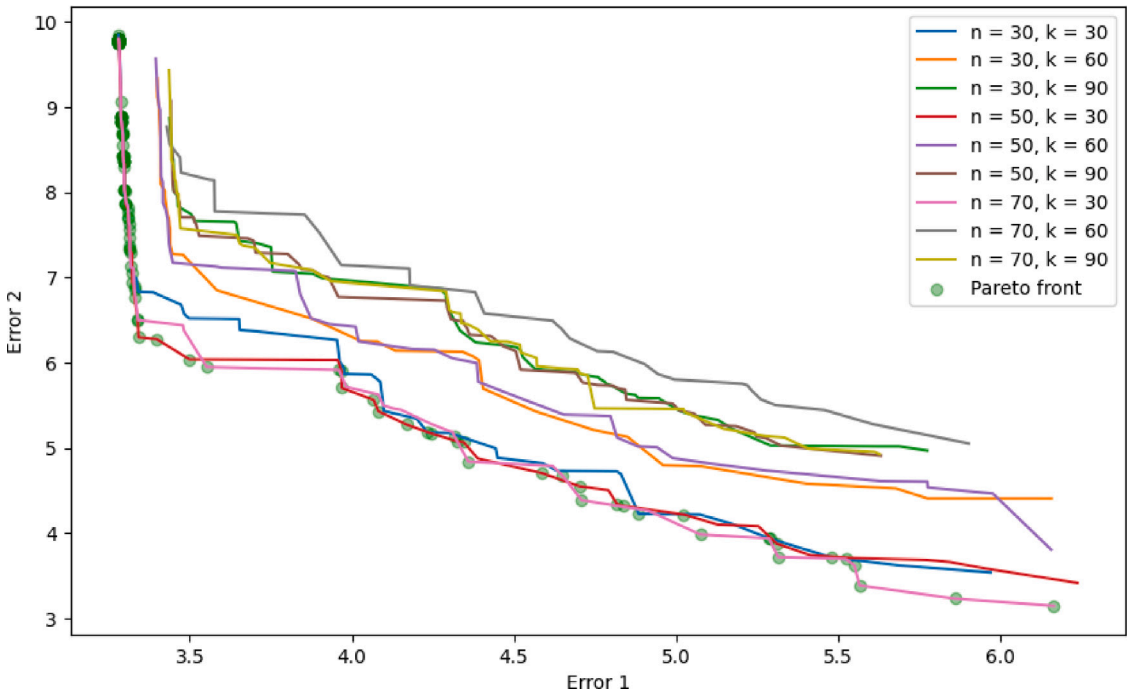

Fig. 6. MOPSO-selection algorithm results and the selected Pareto front.

30, 50, or 70. This gives us 9 combinations of MOPSO-selection algorithm parameters. We run each of them with $s = 9$ for $k = 30$, $s = 15$ for $k = 50$, and $s = 21$ for $k = 70$ (30% in each case) and $ITMAX = 100\,000$ iterations.

We keep the global Pareto-optimal solutions for each of these iterations of the MOPSO-selection algorithm. The results of the 9 Pareto fronts can be seen in Fig. 6. Then out of all these pairs of errors (F_{CI}, F_{IO}) (defined in (9)–(10)), we select the Pareto front, which can be seen as green points in Fig. 6. Each one of these points encodes for $k = 30, 60, 90$ simulations that best explain the uncertainty to produce the Randomized FKPP model based on our algorithmic approach.

Nevertheless, it is convenient to define a criterion to choose only one, although all of them are valid, and the choice of the best one depends on the needs of the study. We choose to select the so-called knee of the Pareto front [43] as illustrated in Fig. 7(a). The knee represents an equilibrium between both errors. This knee encoded for $k = 30$ simulations with 30 associated pairs of parameters (D, r) representing only a small part of the initial 591 pairs as shown in Fig. 7(b).

In Fig. 7(b), the orange points, which represent all the optimal pairs of D and r, exhibit an inverse dependence structure. Moreover, in Fig. 7(c), we can see more blue lines above the NLS estimate than below. This observation suggests that our algorithm tends to favor simulations that exhibit faster growth of CA. Consequently, this preference is likely to shift the distributions of the solutions we will later discuss towards larger values, as depicted in Fig. 9(b).

Let us from now on denote the set of 30 pairs of parameters encoded in the knee as $P_K := \{(D_i, r_i)_{knee}, i = 1, \ldots, 30\}$. Using this set P_K we can visualize how the Randomized FKPP model captures the uncertainty both in 2 and 3 dimensions (later denoted as 2D and 3D, respectively). To represent the Randomized FKPP model in 3D, we will fix a time point $0 < t_0 \leq 48$ ($t = 0$ is excluded since all evaluations have the same IC). We use P_K to get 30 $\hat{u}(x, y, t_0)$ for each point (x, y) in the $[0, 10]^2$ ICU plane. Now, let us denote, for some (x, y), a point in the ICU plane, this set as $U(x, y) = \{\hat{u}_P(x, y, t_0)\}_{P \in P_K}$. Because the distributions of each $U(x, y)$ differ from a normal distribution, we choose not to take the standard 95% CI approximation of [data mean $\pm$ 1.96 data standard deviation] but rather a percentile approach, which is more robust making the 95% CI $\left[Q_{0.025}(U(x, y)), Q_{0.975}(U(x, y))\right]$. The resulting surfaces are illustrated in Fig. 8 for times $t = 5$ h, $t = 10$ h and $t = 20$ h. We can see that the surface of the upper bound of the 95% CI has a longer peak than the mean and lower bound surfaces. This confirms, as previously mentioned, that the mass of the distributions of the solutions for some time t is pulled towards faster growth values.

The estimated distributions of $f(t)$ for $10 < t < 24$ can be represented by using the *ksdensity* function in Matlab. This function provides us with a kernel, a nonparametric representation of the PDF of $f(t)$ at each time point t. The results obtained are represented in Fig. 9(b). We do not show the distributions of $f(t)$ for $t < 10$ and $t > 24$ because all knee simulations converge to the same values there, making the distributions extremely tight and thus clouding the visibility of the time points where distributions are wider. Fig. 9 shows us that most of the data is captured by obtained estimates of the distributions and CIs. Finally, we point out that in the left panel of Fig. 9, we have included the plot for the mean and 95% CI to better compare the results shown in the right panel in the same figure.

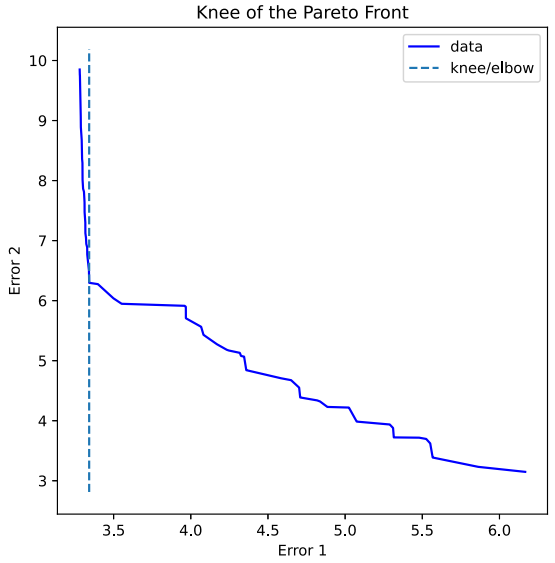

(a) Knee of Pareto front.

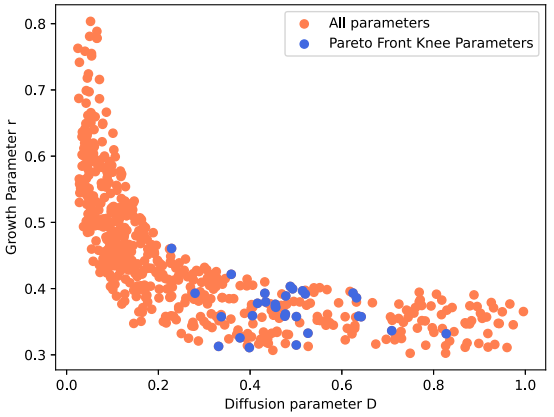

(b) Pairs (D, r) from the 591 initial sets of parameters P_i (in orange) and the selected P_K that best capture the data uncertainty (in blue).

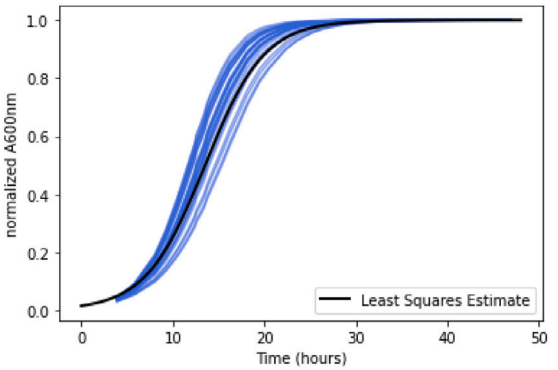

(c) 30 Simulations encoded by the knee of the Pareto front.

Fig. 7. Simulations chosen from the Pareto front to represent the randomness of the model.

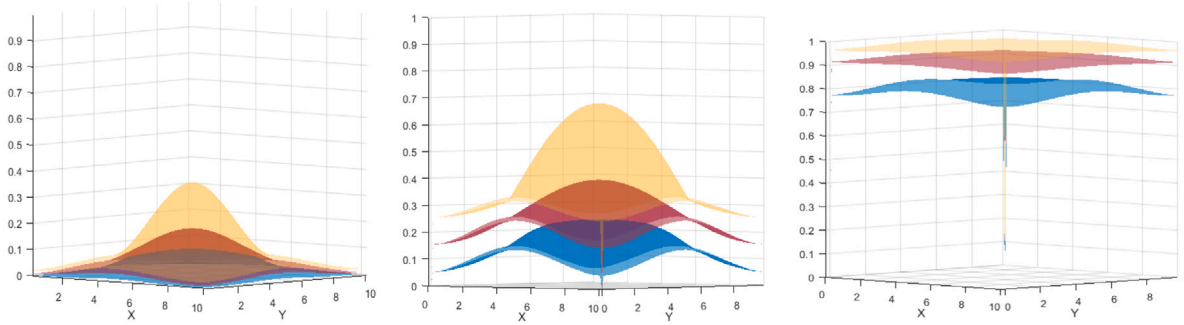

(a) $t = 5h$ (b) $t = 10h$ (c) $t = 20h$

Fig. 8. CA dynamic surfaces with mean (in red) and 95% CI (in blue and yellow).

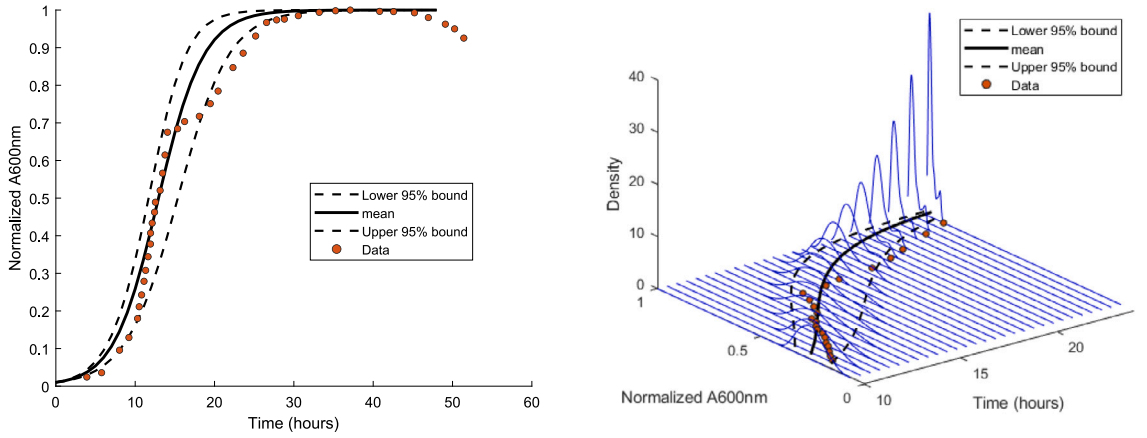

(a) Mean and Confidence Interval for $NormalizedA600nm$.

(b) Densities with 95% CI, mean, and data for hours $10-24$.

Fig. 9. Probability density functions of $A600$ nm and 95% CI with mean.

4.2. Inclusion of cleaning

The cleaning, as defined in Section 2.1, is introduced to simulations generated by the use of the set of parameters P_K that best capture the uncertainty. We choose a cleaning value of p of 0.966 in order to model the efficacy of vaporized hydrogen peroxide (H_2O_2) on CA [44]. H_2O_2 has been recommended in the literature as an efficient cleaning agent to control outbreaks of pathogens [45–47]. It has been indicated to us by ICU medical personnel of Hospital General de Castellón (Spain) that the ICU is cleaned every 8 hours. We thus choose to set $t_1 = 8$ in the cleaning process. We then used the same methodology as mentioned earlier to produce the CI for $f(t)$ values for $0 \le t \le 48$. Fig. 10(a) shows the 30 simulations with cleaning using the parameters pairs from P_K. Note that every 8 hours, there is a vertical line in the plot rather than a jump, which is just a graphical representation choice that allows us to see when cleaning happens clearly. We observe that the pathogen remains under control in almost all the simulations, with its population reaching smaller peaks after each cleaning. However, as can be seen in Fig. 10(a), one simulation of the 30, just before cleaning, has higher peaks as time goes on, implying that CA might not be completely under control. Fig. 10(c) shows the estimated 1-PDF for a given $t = 5, \dots, 40$. Fig. 10(b) shows us 95% CI the built using the 30 selected simulations. We can observe that when the 95% CI is large, the PDF is very wide (platykurtic), and the probability of the values near the upper bound of the CI (which indicates that CA is not under control) is small. This can be interpreted as there is a small probability of CA's population growing fast enough for the homogeneous cleaning with H_2O_2 not being enough to control it. In other words, there is a probability that the pathogen is increasing despite the cleanings. However, the probability that this happens decreases since the mean of each peak decreases, and the 1-PDF flattens over time (as more cleanings are performed).

Fig. 10(b) displays the CI and mean for $f(t)$ obtained by the quantile estimation as mentioned before. It reveals that the simulations consistently indicate population control of CA as the mean and bounds of the CI do not get passed the first peak. It is important to remark that cleaning the entire ICU room uniformly is not possible due to the presence of medical equipment that can only be cleaned with specific cleaning agents that are less efficient against the pathogen in question. Moreover, certain areas throughout the room are difficult to access, posing challenges in cleaning them with the same level of thoroughness as flat surfaces such as floors and tables. Considering these factors, it is important to note that the cleaning strategy employed here is an idealized approach. However, it still serves as a valuable guideline to assess the effectiveness of hydrogen peroxide (H_2O_2) for controlling the CA population.

5. Conclusions

In this work, we proposed a mathematical model to capture the spatial growth of Candida Auris through time. Our model is based on the Fisher Kolmogorov-Petrovky-Piskunov partial differential equation and its numerical solution. To address current health concerns, we have also proposed to include a homogeneous and regular cleaning to model Candida Auris' growth under cleaning pressure.

Then we proposed a computational method to randomize the model. First, we randomized and calibrated the initial model (without cleaning) using *in vitro* Candida Auris growth data. Remarkably, our randomized model fits the data well.

We then included cleaning into the randomized model to observe whether vaporized hydrogen peroxide is effective for Candida Auris population control. We observed that the pathogen's population diminished with every cleaning in all but one of the selected simulations, indicating that the population was under control with significant probability. This suggests that cleaning protocols are

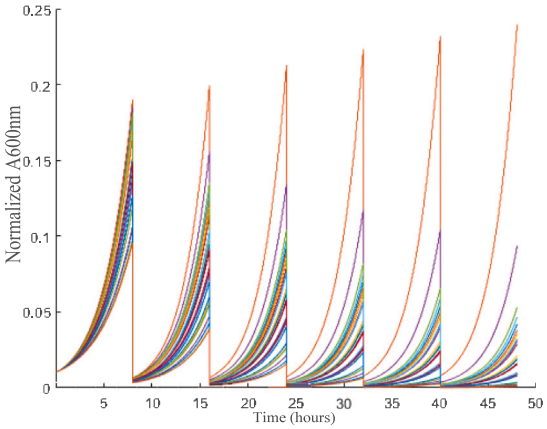

(a) 30 cleaning simulations (each in a different color).

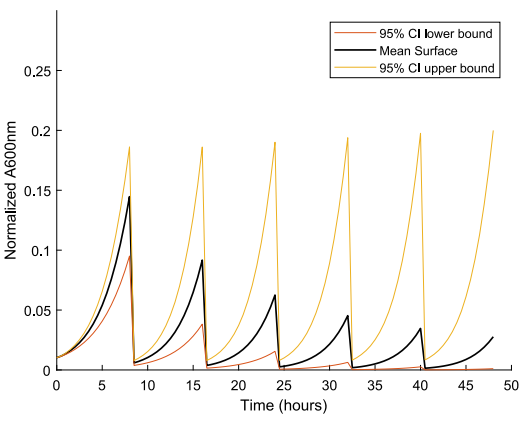

(b) 95% CI built using the 30 cleaning simulations.

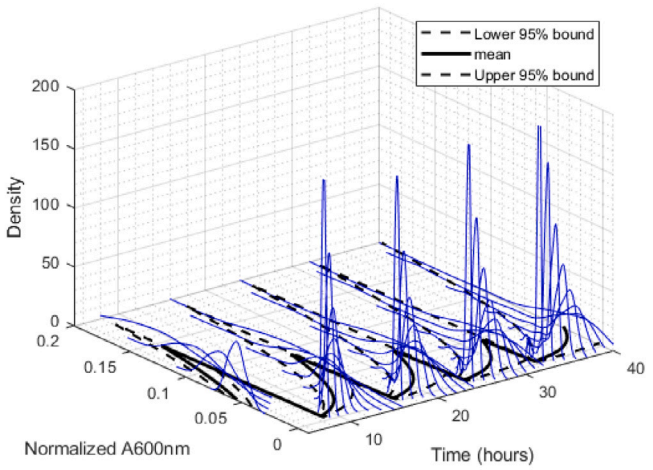

(c) Densities (blue lines) with 95% CI (dotted lines) and mean (solid line).

Fig. 10. Effect of cleaning the ICU room every 8 hours with vaporized H_2O_2.

an effective population control measure for CA; however, it may not be sufficient, and outbreaks with rapid growth may occur, albeit with a very low probability.

The case of uncontrolled growth occurred due to factors that do not impede the pathogen's growth, be it insufficient cleaning. The only factors we control in this model are diffusion (D), growth (r), cleaning efficacy (p), and time in between cleanings (t_1). The model does not give us insight into other factors, and the values we have set for the cleaning factors are the standards used in the Hospital of Castellon and other Spanish Hospitals. Therefore, our goal in this work has been to model what happens in a realistic Intensive Care Unit. We wanted to show why sometimes there is uncontrolled growth of the Candida Auris population when in the Intensive Care Unit, there are strict protocols implemented for cleaning and testing. Furthermore, we tried to explain why such cases happen only sporadically rather than with higher frequency.

There are, however, limitations to this model. First, we used the dataset of *in vitro* growth and not of Candida Auris growing in the Intensive Care Unit. Secondly, Candida Auris competes with many other microorganisms in the Intensive Care Unit environment, and we did not consider this when modeling. Furthermore, it proposes that the Intensive Care Unit is cleaned the same way every time. There are, however, discrepancies in the cleaning thoroughness due to the equipment's peculiarities and human factors.

CRediT authorship contribution statement

Carlos Andreu-Vilarroig: Visualization, Conceptualization, Methodology, Software. **Juan-Carlos Cortés:** Visualization, Writing – review & editing, Writing – original draft, Supervision, Funding acquisition, Project administration. **Cristina-Luisovna Pérez:** Data curation, Investigation, Writing – review & editing, Software, Validation, Conceptualization, Methodology, Formal analysis. **Rafael-Jacinto Villanueva:** Visualization, Supervision, Writing – review & editing, Conceptualization, Methodology, Funding Acquisition, Project administration.

Declaration of competing interest

The authors declare the following financial interests/personal relationships which may be considered as potential competing interests: Cristina Luisovna Perez reports financial support was provided by Government of Spain Ministry of Universities. Juan Carlos Cortes reports financial support was provided by Spanish Agencia Estatal de Investigacion.

Data availability

Data used and its source are specified in the paper

Acknowledgments

This paper has been supported by the Spanish Agencia Estatal de Investigación grant PID2020-115270GB-I00. Cristina Luisovna Pérez has been supported by an FPU21 grant (Formación de Profesorado Universitario 2021) from the Ministerio de Universidades. We want to give our most profound appreciation for the comments and suggestions raised by the two anonymous reviewers who have improved the final version of the paper.

References

[1] Antimicrobial resistance, URL https://www.who.int/news-room/fact-sheets/detail/antimicrobial-resistance, (visited on 07/11/2022)..
[2] R. Wise, Antimicrobial resistance: priorities for action, J. Antimicrob. Chemother. 49 (4) (2002) 585–586, http://dx.doi.org/10.1093/jac/49.4.585.
[3] Franklin D. Lowy, Antimicrobial resistance: the example of staphylococcus aureus, J. Clin. Investig. 111 (9) (2003) 1265–1273, http://dx.doi.org/10.1172/jci18535.
[4] Simona Bungau, Delia Mirela Tit, Tapan Behl, Lotfi Aleya, Dana Carmen Zaha, Aspects of excessive antibiotic consumption and environmental influences correlated with the occurrence of resistance to antimicrobial agents, Curr. Opin. Environ. Sci. Health 19 (2021) 100224.
[5] Kazuo Satoh, et al., Candida auris sp. nov., a novel ascomycetous yeast isolated from the external ear canal of an inpatient in a Japanese hospital, Microbiol. Immunol. 53 (1) (2009) 41–44, http://dx.doi.org/10.1111/j.1348-0421.2008.00083.x.
[6] Anuradha Chowdhary, Cheshta Sharma, Jacquesa F. Meis, Candida auris: a rapidly emerging cause of hospital-acquired multidrug-resistant fungal infections globally, in: Deboraha A. Hogan (Ed.), PLOS Pathogens 13 (5) (2017) e1006290, http://dx.doi.org/10.1371/journal.ppat.1006290.
[7] Nancy A. Chow, Lalitha Gade, Sharon V. Tsay, Kaitlin Forsberg, Jane A. Greenko, Karen L. Southwick, Patricia M. Barrett, Janna L. Kerins, Shawn R. Lockhart, Tom M. Chiller, Anastasia P. Litvintseva, Eleanor Adams, Kerri Barton, Karlyn D. Beer, Meghan L. Bentz, Elizabeth L. Berkow, Stephanie Black, Kristy K. Bradley, Richard Brooks, Sudha Chaturvedi, Whitney Clegg, Melissa Cumming, Alfred DeMaria, Nychie Dotson, Erin Epson, Rafael Fernandez, Tara Fulton, Rebecca Greeley, Brendan Jackson, Alexander Kallen, Sarah Kemble, Monina Klevens, Randy Kuykendall, Ngoc H. Le, Vivian Leung, Emily Lutterloh, Jarred Mcateer, Massimo Pacilli, Joyce Peterson, Monica Quinn, Kathleen Ross, Faye Rozwadowski, D.J. Shannon, Kimberly A. Skrobarcek, Snigdha Vallabhaneni, Rory Welsh, Yan Zhu, Multiple introductions and subsequent transmission of multidrug-resistant Candida auris in the USA: a molecular epidemiological survey, Lancet Infect. Dis. 18 (12) (2018) 1377–1384, http://dx.doi.org/10.1016/s1473-3099(18)30597-8.
[8] Alba Ruiz-Gaitán, Ana M. Moret, María Tasias-Pitarch, Ana I. Aleixandre-López, Héctor Martínez-Morel, Eva Calabuig, Miguel Salavert-Lletí, Paula Ramírez, José L. López-Hontangas, Ferry Hagen, et al., An outbreak due to Candida auris with prolonged colonisation and candidaemia in a tertiary care European hospital, Mycoses 61 (7) (2018) 498–505.
[9] Rory M. Welsh, Meghan L. Bentz, Alicia Shams, Hollis Houston, Amanda Lyons, Laura J. Rose, Anastasia P. Litvintseva, Survival, persistence, and isolation of the emerging multidrug-resistant pathogenic yeast candida auris on a plastic health care surface, in: Daniel J. Diekema (Ed.), J. Clin. Microbiol. 55 (10) (2017) 2996–3005, http://dx.doi.org/10.1128/jcm.00921-17.
[10] Emily Larkin, Christopher Hager, Jyotsna Chandra, Pranab K. Mukherjee, Mauricio Retuerto, Iman Salem, Lisa Long, Nancy Isham, Laura Kovanda, Katyna Borroto-Esoda, Steve Wring, David Angulo, Mahmoud Ghannoum, The emerging pathogen candida auris: Growth phenotype, virulence factors, activity of antifungals, and effect of SCY-078, a novel glucan synthesis inhibitor, on growth morphology and biofilm formation, Antimicrob. Agents Chemother. 61 (5) (2017) http://dx.doi.org/10.1128/aac.02396-16.
[11] Nira Rabin, Yue Zheng, Clement Opoku-Temeng, Yixuan Du, Eric Bonsu, Herman O. Sintim, Biofilm formation mechanisms and targets for developing antibiofilm agents, Future Med. Chem. 7 (4) (2015) 493–512, http://dx.doi.org/10.4155/fmc.15.6.
[12] Johanna Rhodes, Matthew C. Fisher, Global epidemiology of emerging Candida auris, Curr. Opin. Microbiol. 52 (2019) 84–89, http://dx.doi.org/10.1016/j.mib.2019.05.008.
[13] Andrea Cortegiani, Giovanni Misseri, Teresa Fasciana, Anna Giammanco, Antonino Giarratano, Anuradha Chowdhary, Epidemiology, clinical characteristics, resistance, and treatment of infections by candida auris, J. Intensive Care 6 (1) (2018) http://dx.doi.org/10.1186/s40560-018-0342-4.
[14] Davida W. Eyre, et al., A Candida auris outbreak and its control in an intensive care setting, N. Engl. J. Med. 379 (14) (2018) 1322–1331, http://dx.doi.org/10.1056/nejmoa1714373.
[15] U.K. Shyni, R. Lavanya, A study on transmission dynamics of the emerging candida auris infections in intensive care units: Optimal control analysis and numerical computations, Physica A 561 (2021) 125253, http://dx.doi.org/10.1016/j.physa.2020.125253.
[16] Principles of Epidemiology, 2012, URL https://www.cdc.gov/csels/dsepd/ss1978/lesson3/section3.html, (visited on 07/11/2022).
[17] Shabira A. Lone, Aijaz Ahmad, Candida auris–the growing menace to global health, Mycoses 62 (8) (2019) 620–637, http://dx.doi.org/10.1111/myc.12904.
[18] Carmea Salvador García, et al., Candida auris: Descripción de un brote, in: Enfermedades Infecciosas y Microbiología Clínica, 38, 2020, pp. 39–44.
[19] Shyni Unni Kumaran, Lavanya Rajagopal, Optimal control analysis for a Candida auris nosocomial infection model with environmental transmission, Math. Methods Appl. Sci. 45 (11) (2022) 6878–6897.
[20] Amauri J. Paula, Geelsu Hwang, Hyun Koo, Dynamics of bacterial population growth in biofilms resemble spatial and structural aspects of urbanization, Nature Commun. 11 (1) (2020) http://dx.doi.org/10.1038/s41467-020-15165-4.
[21] Vladimir M. Tikhomirov, Selected Works of an Kolmogorov: Volume I: Mathematics and Mechanics, Vol. 25, Springer Science & Business Media, 1991, pp. 242–245.
[22] Leiwen Fu, L. Wang, H. Guo, Z. Liu, J. Yang, Q. Chen, J. Hu, et al., Study on growth characteristics of candida auris under different conditions in vitro and its in vivo toxicity, Zhejiang Da Xue Xue Bao, J. Zhejiang Univ. Med. Sci. 40 (7) (2020) 1049–1055.
[23] John A. Adam, Nicola Bellomo, A Survey of Models for Tumor-Immune System Dynamics, Springer Science & Business Media, 1997.
[24] Fred Brauer, Carlos Castillo-Chavez, Carlos Castillo-Chavez, Mathematical Models in Population Biology and Epidemiology, Vol. 2, (40) Springer, 2012.
[25] Samuel Bernard, Equation FKPP difference finie 2D EXPLICITE, URL https://gist.github.com/samubernard/f989ebc8fde012f53897e6dfe998aace.
[26] Samuel Bernard, Reaction-diffusion PDEs, URL http://math.univ-lyon1.fr/~bernard/3bim_pde.html.

[27] Patrick Lascaux, Lectures on Numerical Methods for Time Dependent Equations: Applications to Fluid Flow Problems, Vol. 52, Tata Institute of Fundamental Research, 1976.
[28] Raina M. Maier, Ian L. Pepper, Bacterial growth, in: Environmental Microbiology, Elsevier, 2015, pp. 37–56.
[29] Douglas M. Bates, Donald G. Watts (Eds.), Nonlinear Regression Analysis and Its Applications, John Wiley & Sons, Inc., 1988, http://dx.doi.org/10.1002/9780470316757.
[30] Douglas M. Bates, Saikat DebRoy, Nonlinear least squares, 2016, URL https://stat.ethz.ch/R-manual/R-devel/library/stats/html/nls.html, (visited on 07/11/2022).
[31] URL https://www.rdocumentation.org/packages/stats/versions/3.6.2.
[32] Åke Björck, Numerical Methods for Least Squares Problems, SIAM, 1996.
[33] J. Kennedy, R. Eberhart, Particle swarm optimization, in: Proceedings of ICNN'95 - International Conference on Neural Networks, IEEE, http://dx.doi.org/10.1109/icnn.1995.488968.
[34] Federico Marini, Beata Walczak, Particle swarm optimization (PSO). a tutorial, Chemometr. Intell. Lab. Syst. 149 (2015) 153–165.
[35] T.T. Soong, Random Differential Equations and Science and Engineering, Academic Press, 1973.
[36] Carlos Andreu-Vilarroig, Juan-Carlos Cortésa, Ana Navarro-Quiles, Sorina-Madalina Sferle, Statistical analysis of a general adsorption kinetic model with randomness in its formulation. An application to real data, MATCH Commun. Math. Comput. Chem. 90 (2023) 19–51, http://dx.doi.org/10.46793/match.90-1.019A.
[37] Juan-Carlos Cortés, Ana Navarro-Quiles, Sorina-Madalina Sferle, Study of nonhomogeneous linear second-order discrete dynamical systems with uncertainties: Solution and stability with applications, Math. Methods Appl. Sci. (2022) http://dx.doi.org/10.1002/mma.8210.
[38] Carlos Andreu-Vilarroig, Josu Ceberio, Juan-Carlos Cortés, Francisco Fernández de Vega, José-Ignacio Hidalgo, Rafael-Jacinto Villanueva, Evolutionary approach to model calibration with uncertainty, in: Proceedings of the Genetic and Evolutionary Computation Conference Companion, ACM, 2022, http://dx.doi.org/10.1145/3520304.3533948.
[39] Yair Censor, Pareto optimality in multiobjective problems, Appl. Math. Optim. 4 (1) (1977) 41–59.
[40] Josu Ceberio, Juan-Carlos Cortés, Francisco Fernández de Vega, Oscar Garnica, J. Ignacio Hidalgo, J. Manuel Velasco, Rafael-Jacinto Villanueva, Approaching epistemic and aleatoric uncertainty with evolutionary optimization: Examples and challenges, in: Proceedings of the Genetic and Evolutionary Computation Conference Companion, Association for Computing Machinery, New York, NY, USA, 2022, pp. 1909–1915, http://dx.doi.org/10.1145/3520304.3533978.
[41] C.A. Coello Coello, Maximino Salazar Lechuga, MOPSO: A proposal for multiple objective particle swarm optimization, in: Proceedings of the 2002 Congress on Evolutionary Computation. CEC'02 (Cat. No. 02TH8600), Vol. 2, IEEE, 2002, pp. 1051–1056.
[42] Clara Burgos, Juan Carlos Cortés, D. Martínez-Rodríguez, Rafael-Jacinto Villanueva, Computational modeling with uncertainty of frequent users of e-commerce in Spain using an age-group dynamic nonlinear model with varying size population, Adv. Complex Syst. 22 (04) (2019) 1950009.
[43] Ville Satopaa, Jeannie Albrecht, David Irwin, Barath Raghavan, Finding a "kneedle" in a haystack: Detecting knee points in system behavior, in: 2011 31st International Conference on Distributed Computing Systems Workshops, IEEE, 2011, pp. 166–171.
[44] Alireza Abdolrasouli, Darius Armstrong-James, Lisa Ryan, Silke Schelenz, In vitro efficacy of disinfectants utilised for skin decolonisation and environmental decontamination during a hospital outbreak with Candida auris, Mycoses 60 (11) (2017) 758–763, http://dx.doi.org/10.1111/myc.12699.
[45] Caroline Blazejewski, Frédéric Wallet, Anahita Rouzé, Rémi Le Guern, Sylvie Ponthieux, Julia Salleron, Saad Nseir, Efficiency of hydrogen peroxide in improving disinfection of ICU rooms, Critical care 19 (2015) 1–8.
[46] A. Chmielarczyk, P.G. Higgins, J. Wojkowska-Mach, E. Synowiec, E. Zander, D. Romaniszyn, T. Gosiewski, H. Seifert, P. Heczko, M. Bulanda, Control of an outbreak of Acinetobacter baumannii infections using vaporized hydrogen peroxide, J. Hosp. Infect. 81 (4) (2012) 239–245.
[47] Jonathan A. Otter, Saber Yezli, Marinus A. Schouten, Arthur R.H. van Zanten, Greetje Houmes-Zielman, Maria K.E. Nohlmans-Paulssen, Hydrogen peroxide vapor decontamination of an intensive care unit to remove environmental reservoirs of multidrug-resistant gram-negative rods during an outbreak, Am. J. Infect. Control 38 (9) (2010) 754–756.